

Geochronology, geochemistry and tectonic significance of the ore-associated granites at the Kaladawan Fe–Mo ore field (Altyn), NW China



Cheng-Ming Wang^a, Li Zhang^{b,*}, Huayong Chen^b, Haoshu Tang^c, Yan-Jing Chen^d, Lian-Hui Dong^e, Xun Qu^e, Yi Zheng^a, Deng-Feng Li^f, Jing Fang^b

^a School of Earth Science and Geological Engineering, Sun Yat-sen University, Guangzhou 510275, China

^b Key Laboratory of Metallogenic Dynamics, Guangzhou Institute of Geochemistry, Chinese Academy of Sciences, Guangzhou 510640, China

^c State Key Laboratory of Ore Deposit Geochemistry, Institute of Geochemistry, Chinese Academy of Sciences, Guiyang 550002, China

^d Key Laboratory of Crust and Orogen Evolution, Peking University, Beijing 100871, China

^e Xinjiang Bureau of Geology and Mineral Resources Exploration and Development, Urumqi 830000, China

^f School of Marine Sciences, Sun Yat-sen University, Guangzhou 510006, China

ARTICLE INFO

Article history:

Received 29 March 2016

Received in revised form 8 May 2017

Accepted 15 May 2017

Available online 19 May 2017

Keywords:

Kaladawan Fe–Mo ore field

Altyn Mountains

Skarn

Highly fractionated I-type granite

Zircon U–Pb and Hf isotopes

ABSTRACT

The Kaladawan Fe–Mo ore field (Altyn, Xinjiang) in Northwest (NW) China contains six deposits, with a total reserve of 60 Mt Fe and 10 Kt Mo metal. The orebodies are hosted in lower Paleozoic andesite, dacite, phyllite and marble with well-developed skarn alteration. The Kaladawan granites are newly U–Pb dated to be Early Ordovician (476.1 ± 3.3 Ma), largely coeval with the Fe–Mo mineralization (molybdenite Re–Os: 480.3 ± 3.2 Ma). The granites contain high SiO₂, K₂O and Al₂O₃, low TiO₂, MgO and CaO, with high K₂O/Na₂O ratios (1.26–1.58) and A/CNK values (1.00–1.08), showing peraluminous high-K calc-alkaline affinity. The rocks are characterized by large ion lithophile element (LILE) and light rare earth element (LREE) enrichments and depletions of Sr, Ba, Nb, Ta, Ti and P, and with negative Eu anomalies. The rocks have initial ⁸⁷Sr/⁸⁶Sr ratios of 0.7066 to 0.7112 and $\epsilon_{\text{Nd}}(t)$ values of –1.4 to –1.1, with $T_{\text{DM2}}(\text{Nd})$ ages of 1.32–1.30 Ga. Zircon $\epsilon_{\text{Hf}}(t)$ values range from 2.9 to 6.4, with $T_{\text{DM2}}(\text{Hf})$ ages of 1.26–1.04 Ga. The new geochemical and isotopic data suggest that the Kaladawan granites are highly fractionated I-type, and likely formed by fractional crystallization of a magma that was derived from partial melting of a mixture of crustal and mantle materials. Deposits in the Kaladawan Fe–Mo field are skarn-type and may have occurred in an active continental margin, via the contact metamorphism and metasomatic reaction between granite-derived fluids and the wall rocks.

© 2017 Published by Elsevier B.V.

1. Introduction

Skarn deposits are one of the most important mineral deposit types worldwide (Einaudi et al., 1981; Meinert et al., 2005). Skarn Fe deposits, locally containing minor Cu, Co, Au, Mo, Pb and Zn (Meinert et al., 2005; Zhang et al., 2014), are the largest skarn deposits (in tonnage). Skarn is featured by the common presence of Ca-silicate minerals (e.g., garnet and diopside), and extensively developed in skarn Fe deposits. Although most skarn Fe deposits are associated with intermediate–felsic intrusions, these intrusions are not prerequisite to form skarn or skarn Fe deposits (Einaudi et al., 1981; Meinert et al., 2005). Thus, the origin of some Fe

deposits associated with extensive skarn developments, especially for those lacking clear spatial link with intrusions, has been widely debated, such as the Mengku deposit in Altay (Wan et al., 2012, 2017), Yamansu Fe deposit in eastern Tianshan in China (Hou et al., 2014b), and some Fe deposits in the Urals, e.g., the Lebyazhinsk Fe deposit (Belevtsev, 1982). In China, some of these deposits have been locally classified as submarine volcanogenic iron-oxide (SVIO), which were defined as volcanic-associated/ volcanic-sedimentary-hosted Fe oxide deposits formed at or near the seafloor in submarine volcanic settings (Hou et al., 2014a; Zhang et al., 2014).

The Kaladawan Fe–Cu–Pb–Zn district is newly discovered in the eastern Altyn Mountains (Xinjiang, NW China) and contains over 14 deposits/prospects, including the Kaladawan Fe–Mo, Baijianshan Fe, Kaladawan Pb–Zn, Kaladaban Pb–Zn deposits/ore fields.

* Corresponding author.

E-mail address: zhangli@gig.ac.cn (L. Zhang).

Most of these deposits are hosted in Paleozoic volcanic–sedimentary rocks, which were intruded by numerous igneous intrusions (Chen et al., 2009; Cui et al., 2010; Hao, 2013). For these Fe polymetallic deposits, their genesis and relationship with nearby intrusions are still poorly understood, which has hampered mineral research and exploration in the region. The Kaladawan Fe–Mo ore field was discovered by the No. 1 Geological Brigade of the Xinjiang Bureau of Geology and Mineral Resources (XJBGMR) in 2006, with a total metal reserve of 60 Mt Fe @ 31.9% and 10 Kt Mo (XJBGMR, 2012). The Kaladawan Fe–Mo mineral systems occur along the intrusive contact between one granite stock and volcanic–sedimentary wall rocks, with the stratiform or lenticular orebodies spatially associated with skarn alteration. The molybdenite in this mineralization has a Re–Os isochron age of 480.2 ± 3.2 Ma (Hao, 2013). Genesis of the Kaladawan ore field was variably argued to be synsedimentary–exhalative with a later hydrothermal overprint (Chen et al., 2009, 2012; Gao et al., 2012; Hao, 2013), SVIO type (Hou et al., 2014a; Zhang et al., 2014) or skarn type (Wang et al., 2014, 2017). The key problem lies in the clarification of spatial, temporal and genetic relationships between mineralization, skarn and the granite stock, which would require more new and precise age, geochemical and mineralogical data.

In this contribution, we report new zircon U–Pb age and Hf isotopes, whole-rock geochemistry and Sr–Nd isotopes for the Kaladawan granites, and discuss the petrogenesis of the granites and their genetic link to the Fe–Mo mineralization. The petrogenesis of the granites can also provide important constraints on the tectonic setting.

2. Geological setting

The Altyn Mountains are situated between the Tarim and Qaidam basins and bounded by the Altyn Fault in the southeast, with the Kaladawan district located in the eastern Altyn Mountains (Fig. 1A and B). The district is suggested to have undergone at least six tectonic episodes: (1) Development of the Archean continental basement; (2) Deposition of the Mesoproterozoic platform sedimentary covers; (3) Neoproterozoic continental rifting and formation of the Altyn Ocean (Chen et al., 2001); (4) Paleozoic subduction and closure of the Altyn Ocean; (5) Mesozoic north-south extension (Chen et al., 2003); (6) Cenozoic strike-slip shearing of the Altyn Fault. Exposed rocks in the district include the Neoproterozoic Milan Complex, Mesoproterozoic Jinyanshan Formation, Neoproterozoic Suoerkuli Group, and the Cambrian Tashibulake, Ordovician Kaladawan and Carboniferous Yingebulake formations. These units are generally folded into the Kaladawan Synclinorium (Hao, 2013).

The Archean Milan Complex is mainly composed of high-grade metamorphic rocks (e.g., granitic gneiss, granulite and migmatite) that are SHRIMP zircon U–Pb dated to be ca. 2830–2567 Ma (Xin, 2012). The Mesoproterozoic Jinyanshan Formation comprises low-grade meta-carbonates intercalated with minor clastic rocks (Hao, 2013), e.g., crystalline limestone, banded siliceous limestone, dolomite, stromatolite-bearing limestone and minor phyllite. The Neoproterozoic Suoerkuli Group is predominately composed of dolomite, calcareous siltstone and oolitic chert. The Tashibulake Formation contains marble, phyllite and minor schist (XJBGMR, 2009). The Kaladawan Formation is dominated by greenschist-facies meta-volcanics, e.g., two mica–quartz schist and chlorite schist (Hao, 2013). The protoliths were suggested to be basalt, basaltic andesite and rhyolitic crystal tuff (Hao, 2013). The Tashibulake Formation hosts the Kaladawan Fe–Mo, Baijianshan Fe and Abei Ag–Pb ore fields/deposits, whereas the Kaladawan Formation hosts the Kaladaban and Kaladawanxian Pb–Zn deposits. The Carboniferous Yingebulake Formation comprises limestone, sandstone and siltstone (Chen et al., 2009; Hao, 2013).

The Kaladawan and Tashibulake formations were intruded by the early Paleozoic granitoids and minor diabase and gabbro. The granitoids include diorite, granodiorite, monzogranite and granite (Han et al., 2012; Meng et al., 2015). Han et al. (2012) divided these Paleozoic intrusive rocks in the Kaladawan district into three episodes: pre-collision (520–500 Ma), syn-collision (490–470 Ma) and post-collision (440–410 Ma).

3. Ore deposit geology

Exposed lithologies in the Kaladawan Fe–Mo ore field include the Cambrian Tashibulake Formation marble, carbonaceous slate, sericite phyllite and schist (Fig. 2). The marble generally occurs as lenses in the schist. The formation was intruded by a gabbro and dolerite dike swarm. Both the Tashibulake Formation and intruding dikes were folded and then intruded by the Kaladawan diorite porphyry, granodiorite and granite. The granite intrusion is E-trending, parallel to the major structural line of the district. Alterations associated with the granite shows a distinct zoning pattern from the granite outward: garnet + pyroxene skarns, to magnetite + molybdenite associated with epidote + actinolite ± tremolite skarns, to epidote + calcite ± wollastonite hornfels (Figs. 3, 4). The majority of magnetite and molybdenite mineralization occurs along the intrusive contact zone and economic molybdenite mineralization only occurs in the west part of the ore field.

The orebodies are mainly S-dipping (dip angle: 50°–85°), contain mainly magnetite and molybdenite with Fe and Mo grades being 20.5–47.2% (average 31.86%) and 0.03–0.16% (average 0.07%), respectively. All the orebodies are hosted in skarns (Fig. 4), and the high grade iron orebodies are usually hosted in retrograde skarns mainly comprising of epidote, tremolite and actinolite. Molybdenite-bearing veins were found crosscutting the magnetite-rich skarn locally. Other ore minerals present include pyrrhotite, pyrite, chalcocopyrite, sphalerite, galena and scheelite. Gangue minerals include garnet, diopside, tremolite, actinolite, epidote, zoisite, chlorite and calcite. Apart for skarn, other common alterations include potassic, silicic, carbonate and chlorite.

Hydrothermal alteration and mineralization at Kaladawan consist of five stages (Stage I–V, Fig. 5): Stage I (prograde skarn): Garnet, pyroxene and minor wollastonite and scapolite occur in the intrusive contact zone between the granites and wall rocks, forming massive skarn. Stage II (retrograde alteration): Amphibole, epidote, zoisite, sphene and apatite, crosscut or partially replace prograde skarn minerals. Stage III (magnetite mineralization): skarn minerals are replaced by magnetite, quartz and epidote. Euhedral to subhedral magnetite occurs as intergrowth with zoisite, or as disseminated or massive aggregates with epidote. Stage IV (sulfide mineralization): Featured by quartz–calcite–sulfide veins crosscutting skarns and generated also magnetite orebodies. Stage V (carbonate and chlorite alterations): Quartz / calcite and calcite–chlorite veins crosscutting previous alteration and mineralization.

4. Samples and analytical methods

4.1. Samples

Due to weathering as well as alteration of the rocks, the least weathered and altered samples of the granite at the 7918 Fe deposit and 7910 Fe–Mo deposit of the Kaladawan field were collected for chemical analysis. Among these, six samples (KFP-2, 4, 6, 7, 11 and 97) from outcrops and two samples (KFP-10 and KFP-8) from drill cores (WZK16401 and WZK16402) (Fig. 4) were used for major and trace elements analysis. The samples KFP-2, KFP-4 and

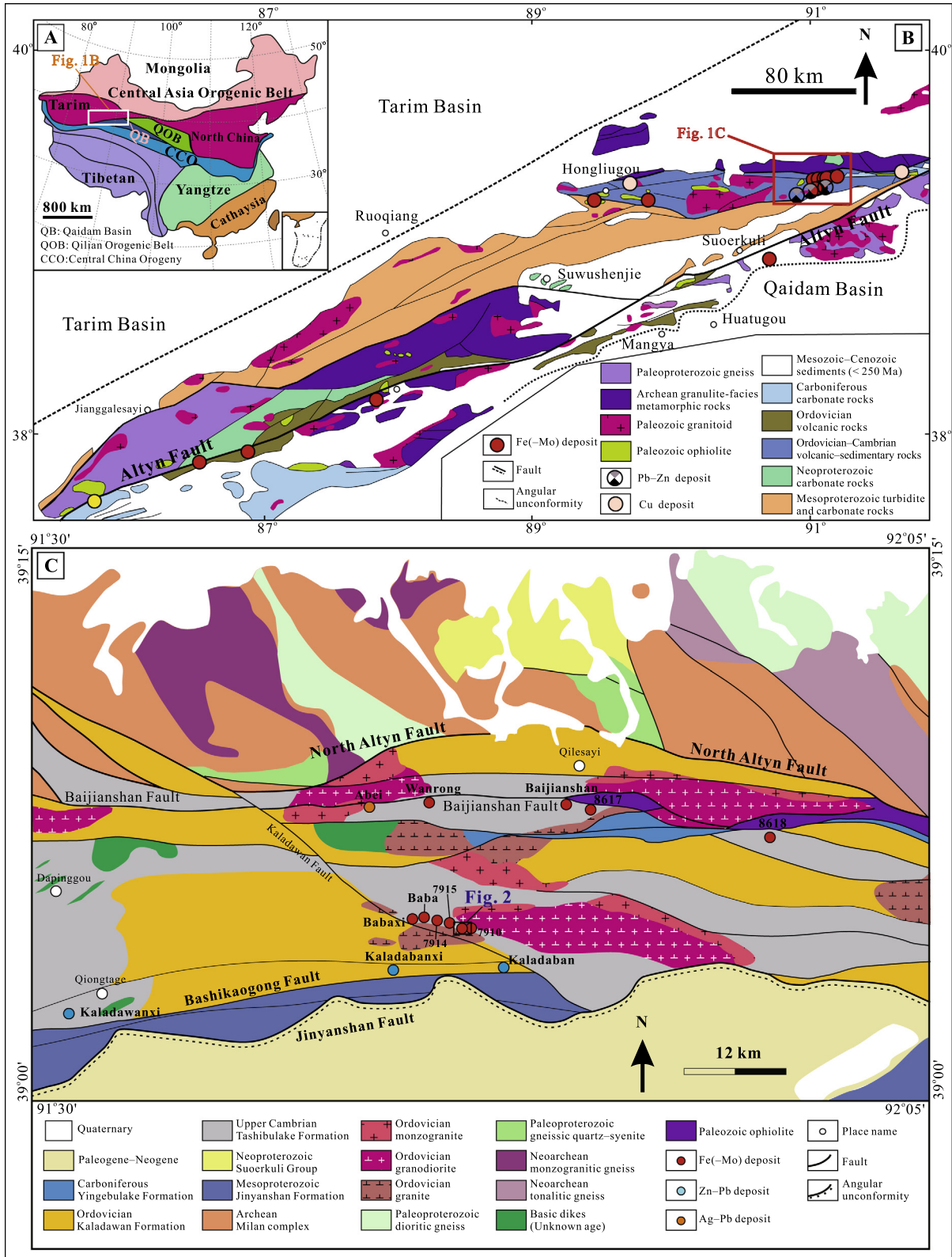


Fig. 1. (A) Tectonic framework of China, showing the location of the Altyn Mountains (modified after Li et al., 2012). (B) Geological map of the Altyn Mountains, showing the location of Kaladawan. (C). Geological map of the Kaladawan ore field, showing the distributions of major Fe–Mo deposits (XBGMR, 2009).

KFP-10 were also used for whole-rock Sr–Nd–Pb isotopic compositions analysis. Zircons from sample KFP-4 were selected for U–Pb dating and Hf isotope analysis.

The granite is pink, fine- to medium-grained (Fig. 6A), and exhibits massive structure and granitic texture (Fig. 6B). It consists of quartz (30%), K-feldspar (40%), plagioclase (25%) and biotite (5%).

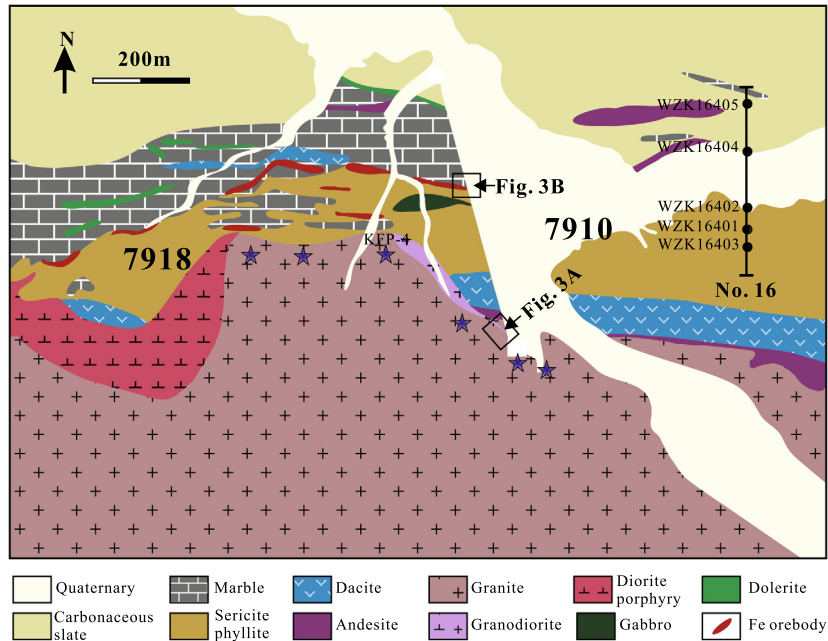


Fig. 2. Geological map of 7918 Fe and 7910 Fe–Mo deposit of the Kaladawan ore field (modified after XBGMR).

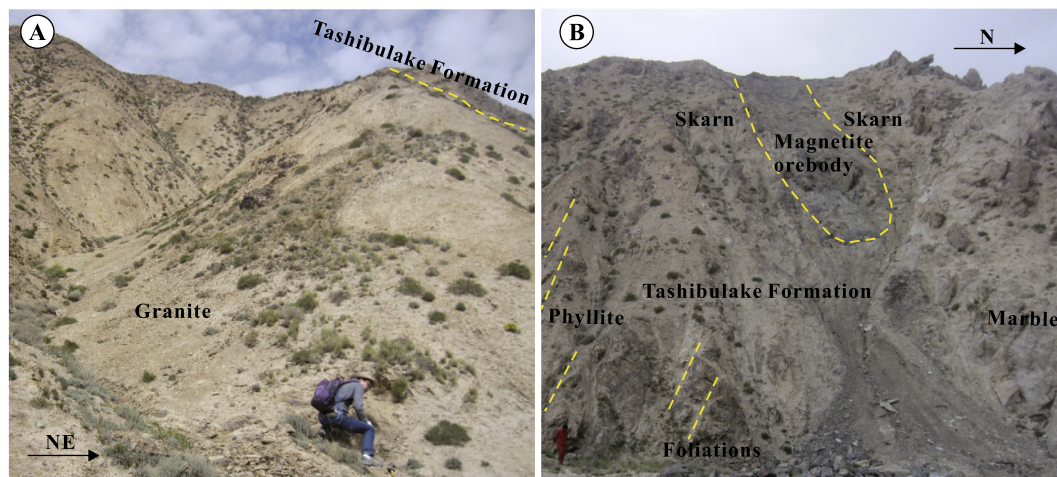


Fig. 3. Field photographs of the Kaladawan ore field. (A) Granite intruded the Tashibulake Formation. (B) Skarn and magnetite orebody.

Biotite is commonly altered into chlorite. The quartz generally shows graphic and myrmekitic texture. Accessory minerals mainly include zircon and magnetite.

4.2. Zircon U–Pb dating

The rock sample was crushed into 80–120 mesh. Zircons were separated with conventional heavy liquid method and the magnetic components were removed with a hand magnet. Zircons were then handpicked under a binocular microscope, mounted in epoxy resin and polished to about half their thickness. Internal structures of the zircons were studied under transmitted light and by cathodoluminescence (CL) imaging.

The selected zircons were analyzed by using the laser ablation inductively coupled plasma mass spectrometry (LA-ICP-MS) at the State Key Laboratory of Continental Dynamics (Northwest University, China) with a GeoLas 200 M system (20 μm laser beam diameter, 10 Hz frequency) coupled with an Agilent 7500a ICP-MS.

Standard reference material SRM610 was used as an external standard for the elements content and ^{29}Si was chosen as an internal standard. Zircon 91500 was used as an external standard for U–Pb dating. The error in the $^{206}\text{Pb}/^{238}\text{U}$ ratio of standard zircons was below 2%. Detailed operating conditions for the laser ablation system and the ICP-MS instrument and data reduction were similar to those described by Liu et al. (2008). Time-drift correction and quantitative calibration for trace element analyses and U–Pb dating were performed by Glitter (ver. 4.0) and the data were reported with a precision of better than $\pm 1\sigma$. Concordia diagrams and weighted average age calculations were made by using Isoplot/Ex_ver3. Weighted average ages for pooled U–Pb analyses were quoted with 95% confidence interval.

4.3. Whole-rock geochemical analysis

Whole-rock major element analysis was performed at the ALS Chemex Laboratory (Guangzhou) by X-ray fluorescence spectrom-

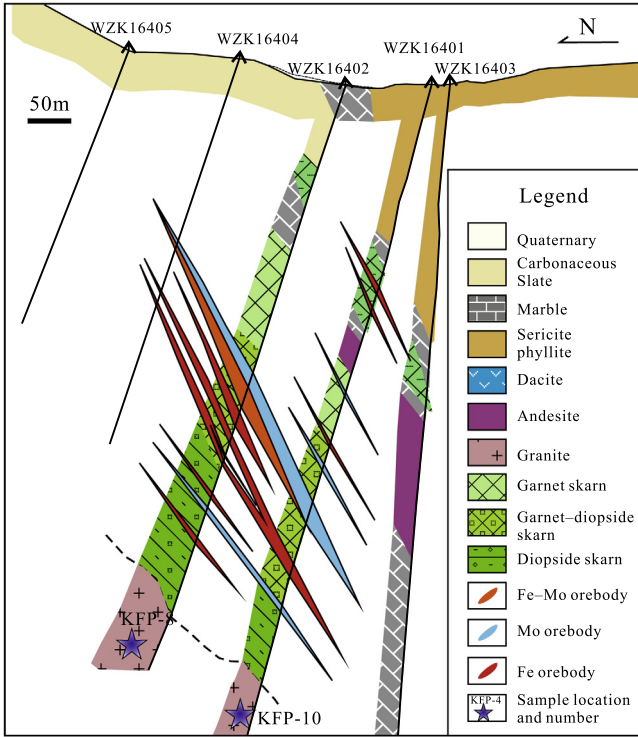


Fig. 4. Geological profile of the No. 16 Prospecting Line.

etry (XRF) on fused glass disks, using the standard GB/T14506.28-1993 for Na₂O, MgO, Al₂O₃, SiO₂, P₂O₅, K₂O, CaO, TiO₂, MnO and Fe₂O_{3T}, standard GB/T14506.2-1993 for H₂O⁺, standard GB

9835–1988 for CO₂ and standard LY/T 1253–1999 for loss-on-ignition (LOI). The precision is estimated to be better than 5%.

Rare earth elements (REEs) and other trace elements (e.g., Cu, Pb, Th, U, Hf, Ta, Sc, Cs, V, Co and Ni) were analyzed by an ELAN6000 ICP-MS at the Analytical Center of Top Resource and Environment (Guiyang), following the procedures of Qi et al. (2000). The standard USGS W-2-G-2 and Chinese Standard GSR-1, GSR-2 and GSR-3 (Govindaraju, 1994) were used to calibrate the element contents, with a precision of better than 3%.

4.4. Whole-rock Sr–Nd isotope analysis

Whole-rock Sr–Nd isotopic analysis was carried out at the State Key Laboratory of Isotope Geochemistry, Guangzhou institute of Geochemistry (GIG), Chinese Academy of Sciences (CAS). The isotopic determination was performed on a Neptune Plus multi-collector (MC)-ICP-MS equipped with nine Faraday cup collectors and eight ion counters. Details of Sr and Nd isotopic analytical methods were similar to those of Deng et al. (2013). Normalizing factors used to correct the mass fractionation of Sr and Nd during the measurements were ⁸⁶Sr/⁸⁸Sr = 0.1194 and ¹⁴⁶Nd/¹⁴⁴Nd = 0.7219. Analyses of the standards NIST SRM987 and Shin Etsu JNdi-1 over the period of measurement yielded ⁸⁷Sr/⁸⁶Sr = 0.710288 ± 0.000005 (2SD) (n = 21) and ¹⁴³Nd/¹⁴⁴Nd = 0.512086 ± 0.000004 (2SD) (n = 19), consistent with the values measured by Weis et al. (2006). The background values of Sr in the process range from 2 × 10⁻¹⁰ to 5 × 10⁻¹⁰, respectively Nd was less than 5 × 10⁻¹¹.

4.5. Zircon Hf isotope analysis

Zircon Hf isotope analysis was carried out in-situ using a Resolution M-50 laser-ablation microprobe, attached to a Neptune Plus MC-ICP-MS at the State Key Laboratory of Isotope Geochemistry,

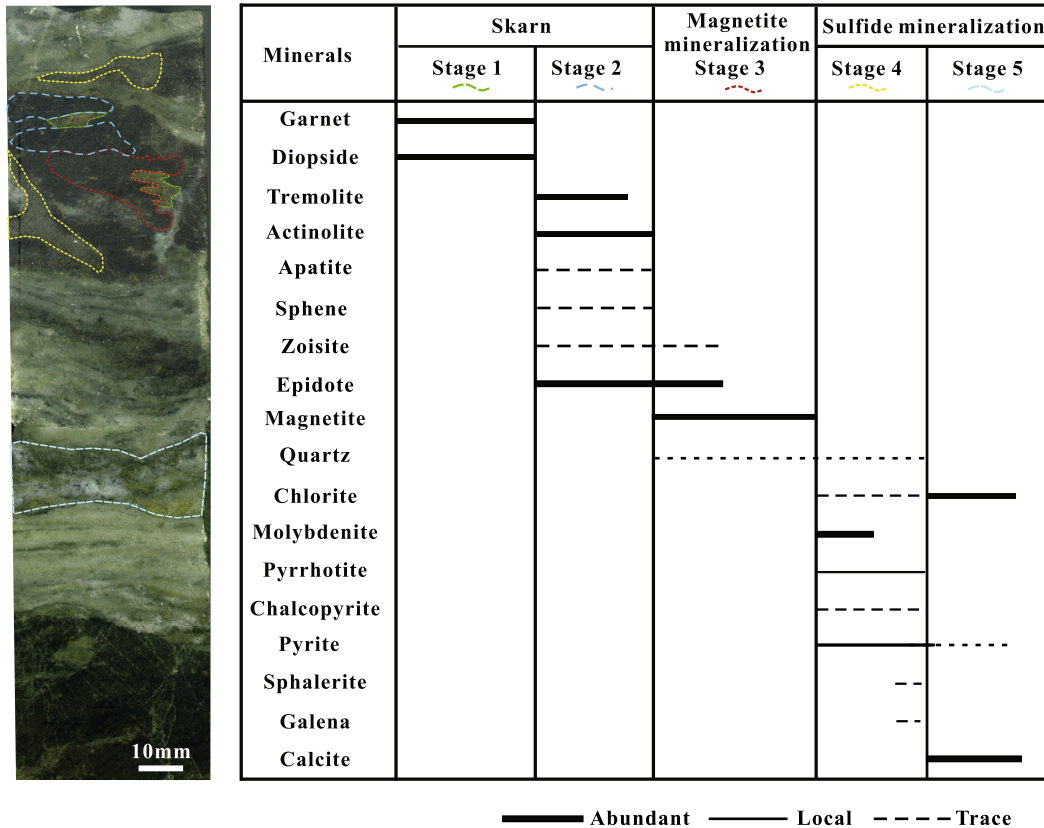


Fig. 5. Alteration and mineralization mineral paragenesis of the Kaladawan Fe–Mo ore field.

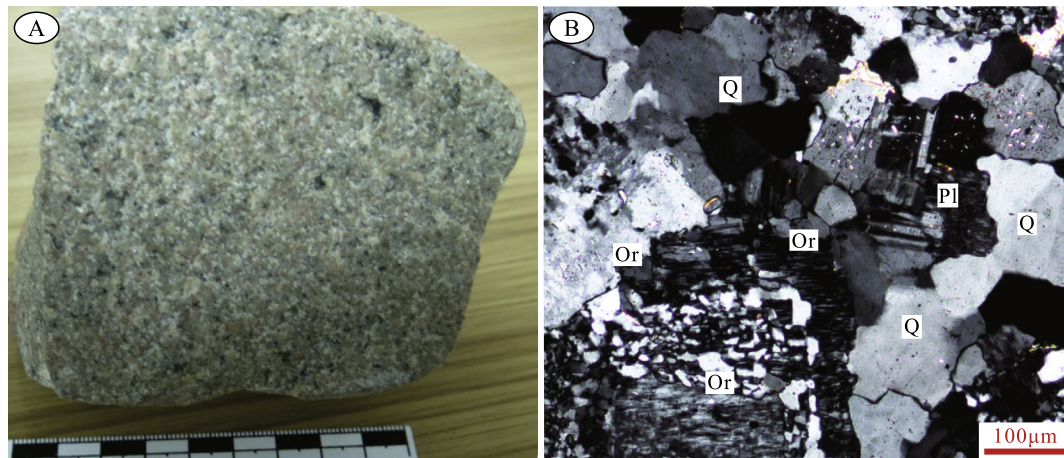


Fig. 6. (A) Hand specimen and (B) thin section (crossed polar) photographs of the Kaladawan granite. Abbreviations: Or: Orthoclase; Q: Quartz; Pl: Plagioclase.

GIGCAS. Instrumental conditions and data acquisition procedures were as described by F.Y. Wu et al. (2006). A stationary spot was used for the present analyses, with a beam diameter of 45 µm. Both He and Ar carrier gases were used to transport the ablated sample from the laser-ablation cell via a mixing chamber to the ICP-MS torch. In order to correct the isobaric interferences of ^{176}Lu and ^{176}Yb on ^{176}Hf , appropriate $^{176}\text{Lu}/^{175}\text{Lu}$ and $^{176}\text{Yb}/^{172}\text{Yb}$ ratios were determined (F.Y. Wu et al., 2006). Zircon Penglai was used as the reference standard, with a weighted mean $^{176}\text{Hf}/^{177}\text{Hf} = 0.282879 \pm 15$ (2σ) yielded by our analyses, consistent with the value of 0.282906 ± 10 yielded from solution analysis by Li et al. (2010).

5. Results

5.1. Zircon U–Pb age and Hf isotopes

Zircon CL images from the granite (KFP-6) show clear and regular oscillatory zoning (Fig. 7A). The zircons are generally colorless transparent, elongated (100–200 µm long; aspect ratios: 1:1 to 2:1) and euhedral prismatic. The 18 analyses yielded U = 566–2561 ppm, Th = 243–1965 ppm, and Th/U = 0.41–1.11 (Table 1). All analyses were plotted on or near the concordia (Fig. 7B) and yielded a weighted average $^{206}\text{U}/^{238}\text{Pb}$ age of 476.1 ± 3.3 Ma (MSWD = 1.8, 2σ) (see Table 1).

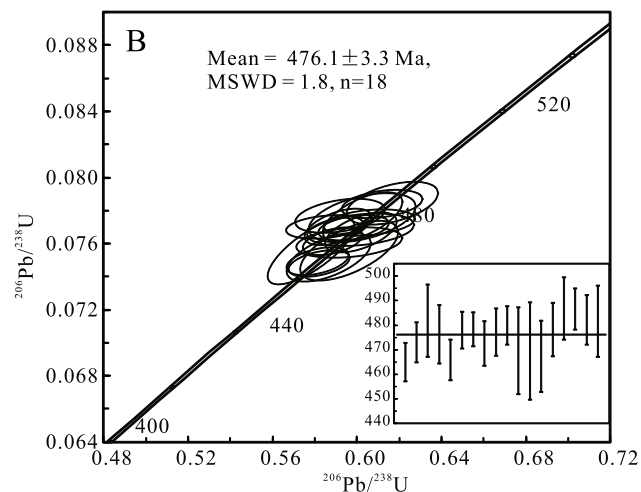
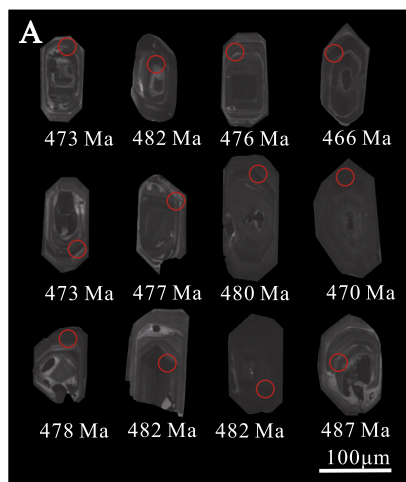


Fig. 7. Zircon CL images and U–Pb concordia diagram for the Kaladawan granite (KFP-4). Red circles indicate the laser spots. (For interpretation of the references to colour in this figure legend, the reader is referred to the web version of this article.)

5.2. Whole-rock geochemistry

5.2.1. Major oxides

The samples are relatively uniform in composition with high SiO_2 (72.87–75.29 wt%, avg. 73.56 wt%), alkali ($\text{Na}_2\text{O} + \text{K}_2\text{O} = 8.59\text{--}9.50$ wt%, avg. 8.97 wt%) and Al_2O_3 (12.99–13.97 wt%, avg. 13.41 wt%), low TiO_2 (0.10–0.19 wt%, avg. 0.15 wt%), MgO (0.10–0.25 wt%, avg. 0.16 wt%) and CaO (0.33–0.87 wt%, avg. 0.63 wt%), belonging to the high-K calc-alkaline series (Fig. 8A; Table 2). The $\text{K}_2\text{O}/\text{Na}_2\text{O}$ ratios and Mg# values are 1.26–1.58 (avg. 1.44) and 12–20 (avg. 15), respectively, whilst the A/CNK and A/NK values are 1.00–1.08 and 1.06–1.23, respectively, indicating a peraluminous nature (Fig. 8B; Table 2).

5.2.2. Trace elements

All the analyzed samples have steep LREE and flat HREE ($(\text{Sm}/\text{Yb})_N = 1.5\text{--}2.5$) chondrite-normalized REE patterns (Fig. 9A). The granites have $\sum\text{REE} + \text{Y} = 186\text{--}311$ ppm, $\sum\text{LREE}/\sum\text{HREE} = 8.1\text{--}12.7$ ($(\text{La}/\text{Yb})_N = 9.6\text{--}16.3$) and $\delta\text{Eu} = 0.19\text{--}0.37$ (Table 2). In the primitive mantle normalized trace element diagrams, these samples show large ion lithophile element (LILE; e.g., Rb and K) enrichment and depletions in Sr, Ba, Nb, Ta, Ti and P (Fig. 9B). They have low Sr (40.3–64.6 ppm) and high Y (26.0–48.2 ppm), yielding low Sr/Y ratios = 1.1–2.0.

Table 1
Results of LA-ICP-MS U–Pb dating for zircons from the Kaladawan granite (KFP-4).

	Th	U	Th/U	²⁰⁷ Pb/ ²⁰⁶ Pb		²⁰⁷ Pb/ ²³⁵ U		²⁰⁶ Pb/ ²³⁸ U		²⁰⁷ Pb/ ²⁰⁶ Pb		²⁰⁷ Pb/ ²³⁵ U		²⁰⁶ Pb/ ²³⁸ U		Concordance
				ppm	ppm	1	Ratio	1σ(%)	Ratio	1σ(%)	Ratio	1σ(%)	Age	1σ	Age	
1	751	1279	0.59	0.0566	1.34	0.5820	2.04	0.0748	0.88	476	25	466	8	465	4	99%
2	1353	2201	0.61	0.0561	1.16	0.5885	1.97	0.0761	0.90	457	26	470	7	473	4	99%
3	612	1069	0.57	0.0564	1.65	0.6026	2.56	0.0776	1.58	478	37	479	10	482	7	99%
4	344	750	0.46	0.0573	1.92	0.6018	2.32	0.0767	1.29	502	43	478	9	476	6	99%
5	1570	2316	0.68	0.0563	1.17	0.5813	2.08	0.0749	0.92	465	31	465	8	466	4	99%
6	978	1548	0.63	0.0565	1.69	0.5983	2.28	0.0770	0.81	472	39	476	9	478	4	99%
7	1965	2561	0.77	0.0549	1.05	0.5847	2.57	0.0770	0.75	409	24	467	10	478	3	97%
8	682	1064	0.64	0.0566	1.79	0.5963	3.44	0.0761	0.99	476	44	475	13	473	5	99%
9	669	1132	0.59	0.0563	1.75	0.6017	3.44	0.0768	1.04	465	34	478	13	477	5	99%
10	1119	1805	0.62	0.0564	1.58	0.6058	2.91	0.0773	0.84	478	35	481	11	480	4	99%
11	804	1439	0.56	0.0568	1.85	0.5963	3.18	0.0756	1.96	483	41	475	12	470	9	98%
12	402	963	0.42	0.0554	1.95	0.5782	2.91	0.0756	2.19	428	47	463	11	470	10	98%
13	1330	1871	0.71	0.0559	1.51	0.5866	2.79	0.0752	1.61	450	35	469	10	467	7	99%
14	1133	1690	0.67	0.0552	1.57	0.5910	2.19	0.0770	1.17	420	35	471	8	478	5	98%
15	243	566	0.43	0.0565	2.26	0.6167	2.87	0.0784	1.35	472	45	488	11	487	6	99%
16	1479	2323	0.64	0.0559	1.18	0.6119	2.56	0.0784	0.90	456	26	485	10	487	4	99%
17	1518	1852	0.82	0.0547	1.64	0.5920	2.95	0.0777	1.08	398	37	472	11	482	5	97%
18	391	784	0.50	0.0561	2.38	0.6025	3.44	0.0776	1.57	457	21	479	13	482	7	99%

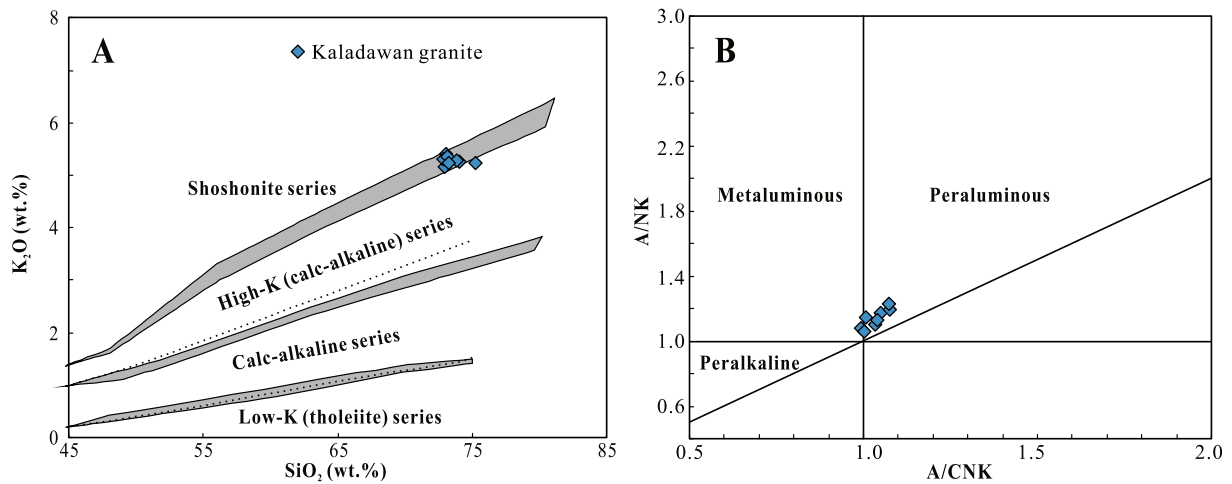


Fig. 8. Granite type discrimination diagrams for the Kaladawan granites.

Table 2
Petrochemical compositions of the Kaladawan granites.

Sample	KFP-2	KFP-4	KFP-6	KFP-7	KFP-8	KFP-10	KFP-11	KFP-97
SiO ₂	74.03	73.05	73.84	72.96	72.87	73.12	73.29	75.29
TiO ₂	0.10	0.13	0.17	0.19	0.19	0.15	0.19	0.10
Al ₂ O ₃	12.99	13.16	13.23	13.81	13.87	13.51	13.68	13.05
Fe ₂ O _{3T}	1.36	2.18	2.24	2.44	2.60	1.83	2.50	1.32
MnO	<0.01	0.01	0.03	0.03	0.02	0.01	0.03	<0.01
MgO	0.10	0.17	0.14	0.25	0.15	0.18	0.18	0.10
CaO	0.48	0.86	0.73	0.87	0.45	0.58	0.72	0.33
Na ₂ O	3.88	3.42	3.37	3.45	4.20	3.73	3.47	4.06
K ₂ O	5.26	5.40	5.28	5.14	5.30	5.35	5.24	5.23
P ₂ O ₅	0.02	0.02	0.01	0.03	0.02	0.02	0.02	0.02
LOI	0.69	0.87	0.51	0.66	0.36	0.54	0.39	0.43
Total	98.90	99.25	99.55	99.84	100.04	99.01	99.70	99.92
Na ₂ O + K ₂ O	9.14	8.82	8.64	8.59	9.50	9.08	8.71	9.29
K ₂ O/Na ₂ O	1.36	1.58	1.57	1.49	1.26	1.43	1.51	1.29
A/(CNK)	1.00	1.01	1.05	1.08	1.03	1.04	1.08	1.01
A/(NK)	1.08	1.15	1.18	1.23	1.10	1.13	1.20	1.06
Mg#	14.63	15.38	12.70	19.55	11.68	18.65	14.12	15.01
Sc	7.26	9.50	12.23	11.79	14.17	7.88	12.76	7.45
V	2.54	3.27	3.45	6.88	3.17	3.63	4.83	1.42
Cr	9.80	4.17	4.11	11.8	4.83	3.92	4.02	3.15
Co	9.16	5.35	2.05	2	2.16	2.60	1.64	1.72
Ni	5.10	2.46	1.58	5.1	1.17	1.94	1.23	2.52
Cu	11.20	7.65	5.79	16.3	2.27	1.22	3.76	8.29
Zn	18.90	21.78	26.9	44.8	18.9	23.58	44.7	24.66

(continued on next page)

Table 2 (continued)

Sample	KFP-2	KFP-4	KFP-6	KFP-7	KFP-8	KFP-10	KFP-11	KFP-97
Rb	169	167	153	159	114	157	163	156
Sr	50.6	62.8	50.8	53.1	40.3	64.6	42.2	41.1
Y	37.9	48.2	35.2	26	28.6	35.6	28.7	34.9
Zr	211	184	198	209	195	203	239	169
Nb	19.4	18.1	17.6	13.9	18.9	14.5	16.7	18.0
Cs	0.18	0.23	0.19	0.26	0.1	0.13	0.36	0.13
Ba	631	729	747	943	1110	1000	891	570
Hf	5.85	4.99	5.53	5.28	5.21	4.94	6.39	4.33
Ta	1.20	1.06	1.31	1.13	1.43	0.70	1.23	0.97
Pb	10.70	13.70	11	8.51	5.94	7.71	9.38	10.90
Th	33.20	32.10	30.44	26.94	25.67	28.90	26.72	26.70
U	3.57	5.55	5.22	3.82	2.94	4.35	4.27	2.89
La	57.30	68.90	60.10	42.40	69.10	53.00	41.80	61.10
Ce	95.50	110.00	98.60	65.70	98.70	88.10	67.40	103.00
Pr	9.93	11.40	10.40	7.06	11.30	9.47	7.67	10.50
Nd	31.80	36.20	32.90	23.30	34.20	31.00	25.30	34.10
Sm	5.92	6.77	6.09	4.28	5.30	5.62	4.64	6.09
Eu	0.36	0.43	0.42	0.51	0.49	0.54	0.48	0.38
Gd	5.47	7.01	5.85	4.22	4.82	5.12	4.56	5.66
Tb	0.99	1.27	0.95	0.68	0.72	0.89	0.76	0.91
Dy	5.73	7.47	5.70	4.17	4.08	5.00	4.70	4.98
Ho	1.18	1.56	1.16	0.87	0.84	1.03	1.00	1.01
Er	3.62	4.87	3.67	2.70	2.71	3.11	3.12	3.04
Tm	0.52	0.74	0.52	0.41	0.43	0.46	0.48	0.43
Yb	3.39	4.97	3.67	2.91	3.10	3.08	3.12	2.69
Lu	0.49	0.73	0.55	0.43	0.50	0.47	0.47	0.39
∑REE + Y	260.10	310.52	265.77	185.64	264.89	242.49	194.20	269.18
δEu	0.19	0.19	0.21	0.37	0.29	0.30	0.31	0.19
(La/Yb) _N	12.12	9.94	11.75	10.45	15.99	12.34	9.61	16.29

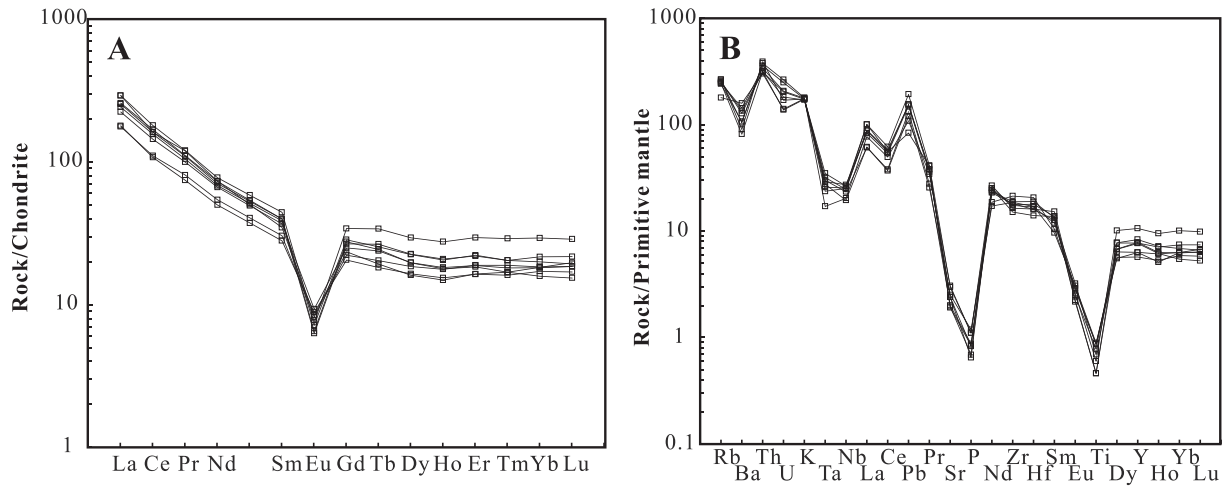


Fig. 9. (A) Chondrite-normalized REE patterns and (B) primitive mantle-normalized multi-element diagrams for the Kaladawan granites. Normalization values are from Sun and McDonough (1989).

5.3. Whole rock Sr–Nd isotopes

Ratios of $^{87}\text{Rb}/^{86}\text{Sr}$ and $^{147}\text{Sm}/^{144}\text{Nd}$ were calculated using the Rb, Sr, Sm and Nd concentrations obtained by ICP-MS and the measured isotope ratios of the samples. The initial $^{87}\text{Sr}/^{86}\text{Sr}$ ratio was calculated using $\lambda_{\text{Rb}} = 1.42 \times 10^{-11} \text{ a}^{-1}$ (Steiger and Jäger, 1977). The $\varepsilon_{\text{Nd}}(t)$ value was calculated using $(^{143}\text{Nd}/^{144}\text{Nd})_{\text{CHUR}} = 0.512638$, $(^{147}\text{Sm}/^{144}\text{Nd})_{\text{CHUR}} = 0.1967$ (Jacobsen and Wasserburg, 1980) and $\lambda_{\text{Sm}} = 6.54 \times 10^{-12} \text{ a}^{-1}$ (Lugmair and Marti, 1978). The $T_{\text{DM1}}(\text{Nd})$ was calculated using $(^{143}\text{Nd}/^{144}\text{Nd})_{\text{DM}} = 0.51315$ and $(^{147}\text{Sm}/^{144}\text{Nd})_{\text{DM}} = 0.2137$ (Peucat et al., 1988). Age used in the calculations is 476.1 Ma. The samples have $^{87}\text{Rb}/^{86}\text{Sr} = 7.06\text{--}9.73$ and $(^{87}\text{Sr}/^{86}\text{Sr})_i = 0.7066\text{--}0.7112$. Their $\varepsilon_{\text{Nd}}(t)$ and $T_{\text{DM2}}(\text{Nd})$ are -1.4 to -1.1 and $1.32\text{--}1.30$ Ga, respectively (Table 3).

Table 3

Whole-rock Sr–Nd isotopic compositions of the Kaladawan granites.

	KFP-2	KFP-4	KFP-10
Age (Ma)	476.1 Ma	476.1 Ma	476.1 Ma
Rb/ppm	169	167	157
Sr/ppm	50.6	62.8	64.6
Rb/Sr	3.34	2.66	2.43
$^{87}\text{Sr}/^{86}\text{Sr}$	0.777192	0.762029	0.754506
2σ	0.000006	0.000006	0.000005
$^{87}\text{Rb}/^{86}\text{Sr}$	9.73	7.74	7.06
$(^{87}\text{Sr}/^{86}\text{Sr})_i$	0.7112	0.7096	0.7066
Sm/ppm	5.92	6.77	5.62
Nd/ppm	31.8	36.2	31.0
$^{143}\text{Nd}/^{144}\text{Nd}$	0.512313	0.512320	0.512293
2σ	0.000003	0.000004	0.000003
$^{147}\text{Sm}/^{144}\text{Nd}$	0.11	0.11	0.11
$C_{\text{Nd}}(t)$	-1.2	-1.1	-1.4
$T_{\text{DM1}}(\text{Ga})$	1.26	1.26	1.25
$T_{\text{DM2}}(\text{Ga})$	1.31	1.30	1.32

Table 4

Zircon Hf isotope data for the Kaladawan granite (KFP-4).

Sample	Age(Ma)	$^{176}\text{Yb}/^{177}\text{Hf}$	$^{176}\text{Lu}/^{177}\text{Hf}$	$^{176}\text{Hf}/^{177}\text{Hf}$	2σ	$(^{176}\text{Hf}/^{177}\text{Hf})_i$	$\varepsilon\text{Hf}(0)$	$\varepsilon\text{Hf}(t)$	$T_{\text{DM}}(\text{Ga})$	$T_{\text{DM},2}(\text{Ga})$	$f_{(\text{Lu}/\text{Hf})}$
KFP-4-4	481.9	0.081706	0.002300	0.282658	0.000015	0.282637	-4.0	5.8	0.87	1.08	-0.93
KFP-4-5	476.3	0.131000	0.003619	0.282689	0.000016	0.282657	-2.9	6.4	0.86	1.04	-0.89
KFP-4-8	477.9	0.086151	0.002436	0.282661	0.000015	0.282640	-3.9	5.8	0.87	1.08	-0.93
KFP-4-10	478.3	0.162139	0.004772	0.282611	0.000017	0.282568	-5.7	3.3	1.01	1.24	-0.86
KFP-4-11	472.6	0.056918	0.001677	0.282582	0.000017	0.282567	-6.7	3.2	0.97	1.24	-0.95
KFP-4-13	477.2	0.057421	0.001634	0.282628	0.000014	0.282614	-5.1	4.9	0.90	1.14	-0.95
KFP-4-16r	469.5	0.080872	0.002301	0.282582	0.000013	0.282562	-6.7	2.9	0.98	1.26	-0.93
KFP-4-18	478.3	0.107039	0.002835	0.282606	0.000013	0.282581	-5.9	3.8	0.96	1.21	-0.91
KFP-4-20	486.6	0.115433	0.003082	0.282584	0.000013	0.282556	-6.6	3.1	1.00	1.26	-0.91

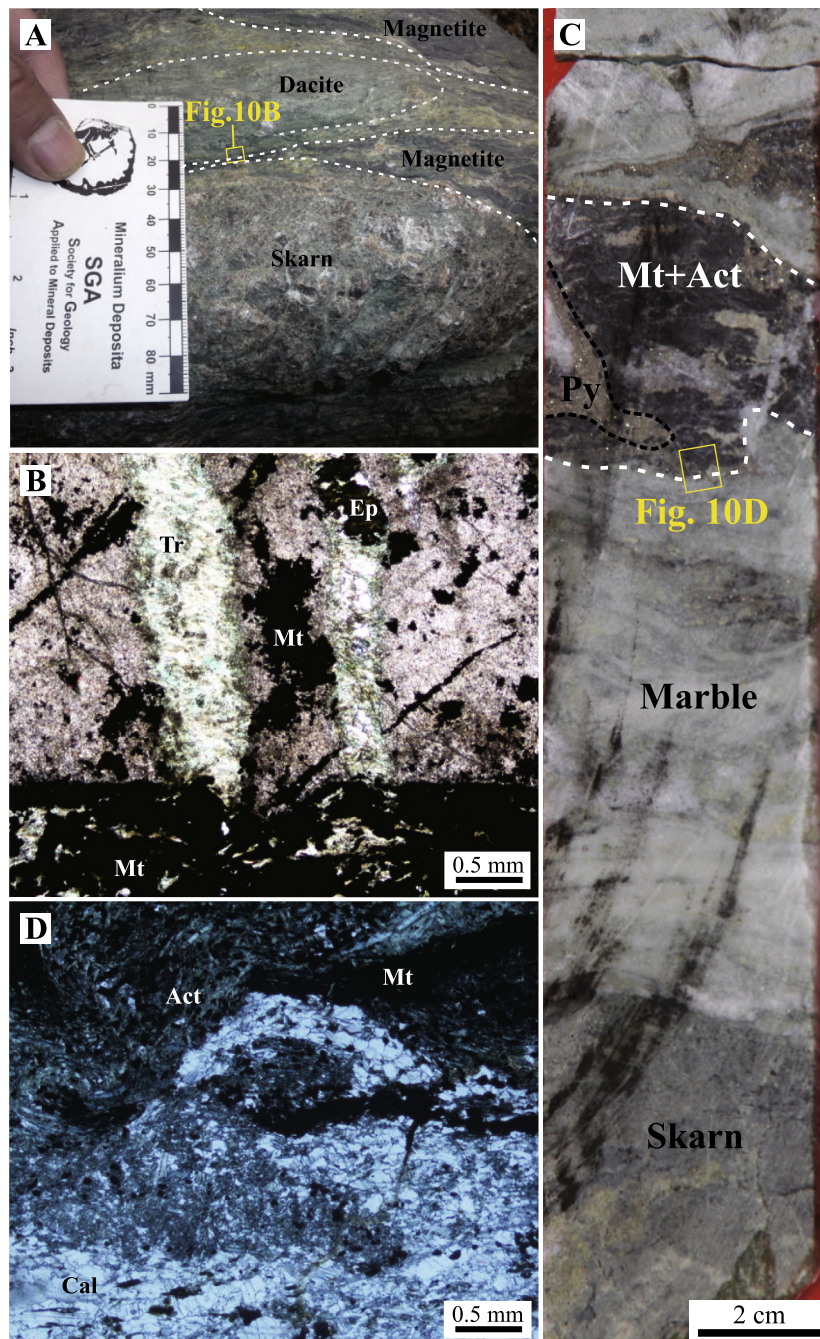


Fig. 10. Photographs showing crosscutting relationships between the skarn and (A, B) volcanic rocks and (C, D) marble from the Kaladawan ore field. Abbreviations: Act: Actinolite; Cal: Calcite; Ep: Epidote; Mt: Magnetite; Py: Pyrite; Tr: Tremolite.

5.4. Zircon Hf isotopes

The decay constant for ^{176}Lu was adopted to be 1.865×10^{-11} year $^{-1}$ (Scherer et al., 2001). Initial $^{176}\text{Hf}/^{177}\text{Hf}$ ratios and $\varepsilon_{\text{Hf}}(t)$ were calculated with reference to the chondritic reservoir (CHUR) at the time if zircon crystallized from magmas, the chondritic $^{176}\text{Hf}/^{177}\text{Hf}$ ratio of 0.282772 and $^{176}\text{Lu}/^{177}\text{Hf}$ ratio of 0.0332 are from Blichert-Toft and Albarède (1997). Single-stage model ages (T_{DM1}) were calculated with reference to the depleted mantle at a present-day $^{176}\text{Hf}/^{177}\text{Hf}$ ratio of 0.28325, similar to that of the average MORB (Nowell et al., 1998) and $^{176}\text{Lu}/^{177}\text{Hf} = 0.0384$ (Griffin et al., 2000). Two-stage model ages (T_{DM2}) were calculated assuming a $^{176}\text{Lu}/^{177}\text{Hf} = 0.015$ for the average continental crust (Griffin et al., 2002).

Zircons from the Kaladawan granite have $^{176}\text{Lu}/^{177}\text{Hf}$ and $^{176}\text{Hf}/^{177}\text{Hf}$ of 0.001634–0.004772 and 0.282582–0.282689, respectively. The calculated $\varepsilon_{\text{Hf}}(t)$, $f_{\text{Lu/Hf}}$ and T_{DM2} ages are of 2.9–6.4, –0.95 to –0.86 and 1.26–1.04 Ga, respectively (Table 4).

6. Discussion

6.1. Age and genesis of the Kaladawan Fe–Mo mineralization

In this study, a new zircon U–Pb age of the Kaladawan granite yielded 476.1 ± 3.3 Ma, consistent with the mineralization age (molybdenite Re–Os: 480.2 ± 3.2 Ma) reported by Hao (2013), suggesting that both the granite magmatism and mineralization at Kaladawan occurred in the Early Ordovician.

The origin of the Fe mineralization at Kaladawan remains controversial. Some authors proposed that the Fe mineralization is syn sedimentary–exhalative type (resembling SEDEX) while the Mo mineralization would have been caused by contact metasomatism during the Kaladawan granite emplacement (Chen et al., 2009, 2012; Gao et al., 2012; Hao, 2013). Some other authors suggested a submarine volcanogenic iron oxide (SVIO)-type (Hou et al., 2014a; Hou et al., 2014b; Zhang et al., 2014). However, the absence of primary hematite, Fe-hydroxides, carbonates and exhalite (e.g., chert) is inconsistent with a synsedimentary–exhalative origin of the Fe mineralization (Dill, 2010). Furthermore, geological and geochemical evidence suggests that these deposits are skarn deposits: (1) All the orebodies are controlled by skarns rather than the volcanic or sedimentary rocks of the Tashbulake Formation: The volcanic and sedimentary rocks were either intruded or replaced by

skarn minerals (Fig. 10), and then followed by magnetite and sulfide mineralization. This indicates that the mineralization is younger than the wall rocks; (2) The Fe–Mo mineralization was coeval with the granite emplacement, and the skarn zonation pattern also indicates that the Kaladawan granites provided the heat and fluids. The occurrence of a causative pluton is in strong contrast with a SVIO origin (Hou et al., 2014a; Hou et al., 2014b); (3) Prograde-stage minerals, e.g., diopside and garnet, were replaced by retrograde-stage epidote – actinolite assemblages. The skarn alteration was overprinted by magnetite and sulfide mineralization. This temporal evolution is similar to those of typical skarn deposits (Meinert et al., 2005); (4) Pyroxene at Kaladawan contains more diopside than hedenbergite (55.4–94.7 mol% diopside; 42.5–4.7 mol% hedenbergite) and garnet is dominated by andradite with minor grossular (61.2–94.4 mol% andradite; 37.5–5.0 mol% grossularite; Wang et al., 2017). This is different from the garnet of a syn sedimentary–exhalative origin (including SVIO), which are featured by Mn- and Fe-rich spessartine and almandine (Burton et al., 1999; Hou et al., 2014b); (5) The Kaladawan magnetite has unusually high Mg, Mo and Cr contents, and its (Ti + V) and (Al + Mn) values are similar to typical skarn Fe mineralization but distinct from SVIO- or BIFs-type mineralization (Wang et al., 2017). In summary, the deposits in Kaladawan ore field are similar to typical skarn deposits, like those in the Yangtze River Valley metallogenic belt, e.g., Chengchao Fe deposit (Mao et al., 2011; Pan and Dong, 1999; Zhai et al., 1996), the Shangfanggou Mo–Fe deposit in Eastern Qinling (Yang et al., 2013) and the Vegas Peledas skarn Fe deposit in Argentina (Pons et al., 2009). The genetic mechanism of the deposits at Kaladawan may have been similar to genetic models of typical skarn deposits associated with felsic intrusions (Einaudi et al., 1981; Meinert et al., 2005): During the Kaladawan granites emplacement, the initial high-temperature contact metamorphism and bimetasomatism may have generated the epidote hornfels and garnet–pyroxene prograde skarn. With the cooling of the pluton and possible circulation of meteoric water (Wang, et al., 2014), replacement of prograde skarn minerals by the actinolite – epidote retrograde assemblage may have caused the precipitation of magnetite and sulfide minerals.

6.2. Magma source and petrogenesis of the Kaladawan granites

Granitic rocks are commonly divided into I-, S-, M-, and A-types according to their source-rocks (Pitcher, 1982). The Kaladawan

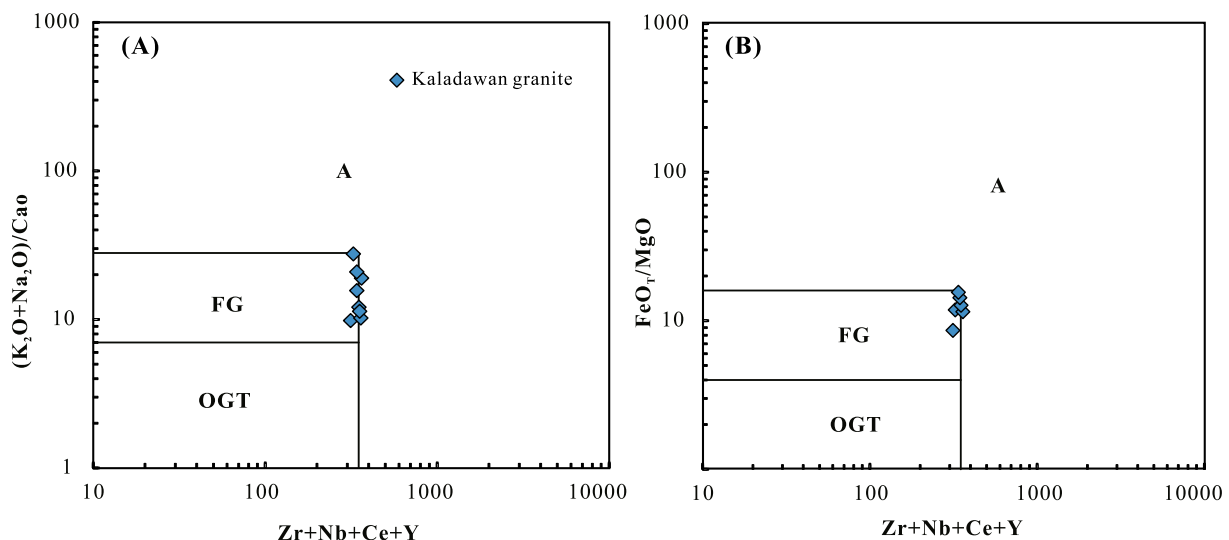


Fig. 11. (A) $(\text{K}_2\text{O} + \text{Na}_2\text{O})/\text{CaO}$ and (B) FeO_7/MgO vs. $(\text{Zr} + \text{Nb} + \text{Ce} + \text{Y})$ (Whalen et al., 1987) granite classification diagrams for the Kaladawan granites. Abbreviations: A: A-type; I, S & M: M-, I- and S-type granites; FG: Fractionated granites; OGT: Unfractionated M-, I- and S-type granites.

granites are unlikely to be M-type, which comprises mainly quartz and plagioclase, and is characterized by low K as well as K_2O/Na_2O ratios (<1 , Coleman and Donato, 1979). The Kaladawan granites contain relatively low Zr, Nb and Y, as well as low 10000 Ga/Al values (2.01–2.53) and (Zr + Nb + Ce + Y) values (300.70–344.40 ppm, Fig. 11A, B), suggesting that they are not A-type either. The high SiO_2 (72.87–75.29 wt%) and alkalis ($Na_2O + K_2O = 8.59–9.50$ wt%), low TiO_2 (0.10–0.19 wt%), MgO (0.10–0.25 wt%) and CaO (0.33–0.87 wt%), and Ba, Sr, Nb, P and Eu depletions of the granites suggest significant fractional crystallization (Wu et al., 2003), are all indicative that the Kaladawan granites fall into the highly fractionated granite field in the discrimination diagrams (Fig. 11A, B). The contrasting behavior of P_2O_5 is a simple indicator of I- or S-type character among the fractionated felsic granites (Chappell and White, 1992; Chappell, 1999). The P_2O_5 content in S-type granites increases or remains unchanged when SiO_2 content increases, whereas P_2O_5 and SiO_2 contents in I-type granites are negatively correlated (Chappell and White, 1992). The Kaladawan granites have low P_2O_5 (0.01–0.03%), negative P_2O_5 vs. SiO_2 correlation but positive Rb vs. Y correlation (Fig. 12A, B), indicating that the granites are highly fractionated I-type (Chappell and White, 1992; Li et al., 2007).

The protoliths of I-type granite are mainly igneous rocks from crust (Chappell and White, 1992). Thus, the Kaladawan granites were likely sourced from crustal materials. They belong to peraluminous high-K calc-alkaline series (Fig. 8), characterized by enrichment in LILEs (e.g., Rb and K), Pb and LREE and depletion in HFSEs (e.g., Nb, Zr, P and Ti) and HREE (Fig. 9), demonstrating the features of igneous rocks related to oceanic plate subduction (Pearce and Norry, 1979; Pearce and Peate, 1995; Stern et al., 2003). The development of contemporary mafic-intermediate rocks in the Kaladawan district (Chen et al., 2016; Cui et al., 2010) implies that all these rocks were the products of partial melting of the lower crust and/or mantle wedge mantle, with addition of water and/or melt sourced from the subducted oceanic slab (Pearce and Peate, 1995; Zheng et al., 2015). The positive $\epsilon_{Hf}(t)$ values (2.9–6.4) also indicate a source of depleted mantle materials (Fig. 13A). Petrogenetic modeling was undertaken to test this hypothesis, using the values of depleted mantle (DM) to represent the mantle source and the Mesoproterozoic basalt of Altyn Mountains to represent the lower crust (LC). Based on these starting materials the Sr and Nd isotopic data show that the Kaladawan granites can be generated by mixture ratios (LC melt to DM melt) from 15:85 to 40:60 with an average of 28:72 (Fig. 13B). And the granite shows positive

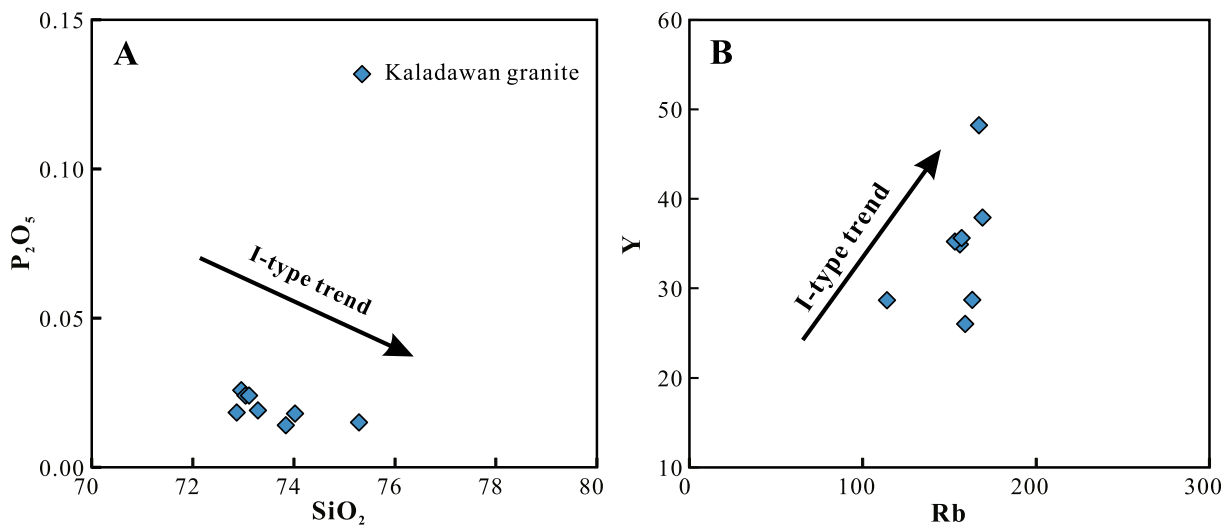


Fig. 12. (a) P_2O_5 vs. SiO_2 (Chappell and White, 1992) and (b) Y vs. Rb diagrams for the Kaladawan granites.

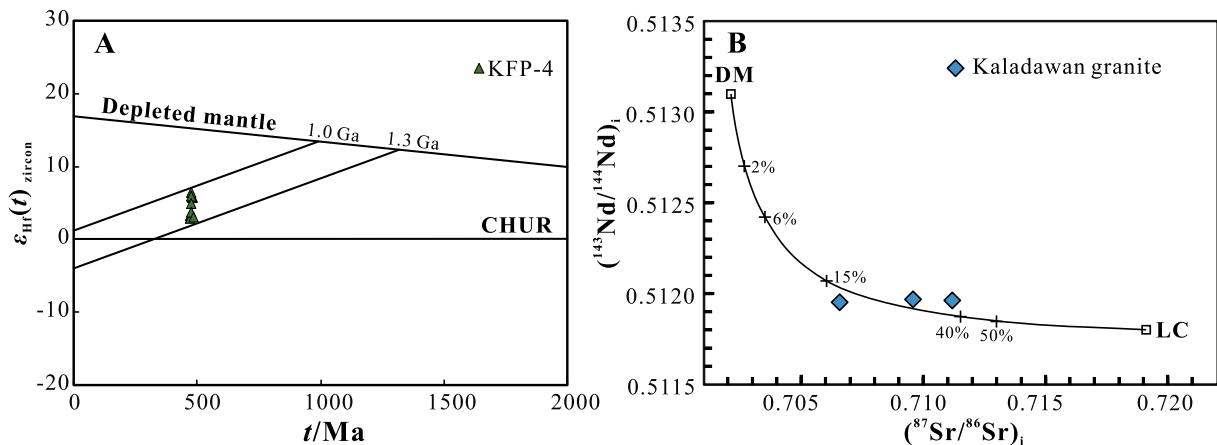


Fig. 13. (A) Diagrams of zircon $\epsilon_{Hf}(t)$ vs. ages and $(^{87}Sr/^{86}Sr)_i$ vs. $\epsilon_{Nd}(t)$ diagram for the Kaladawan granites. The Sr–Nd isotopic compositions of depleted mantle are from Salters and Stracke (2004) and the Mesoproterozoic basalt of Altyn Mountains are from Che et al. (1995b).

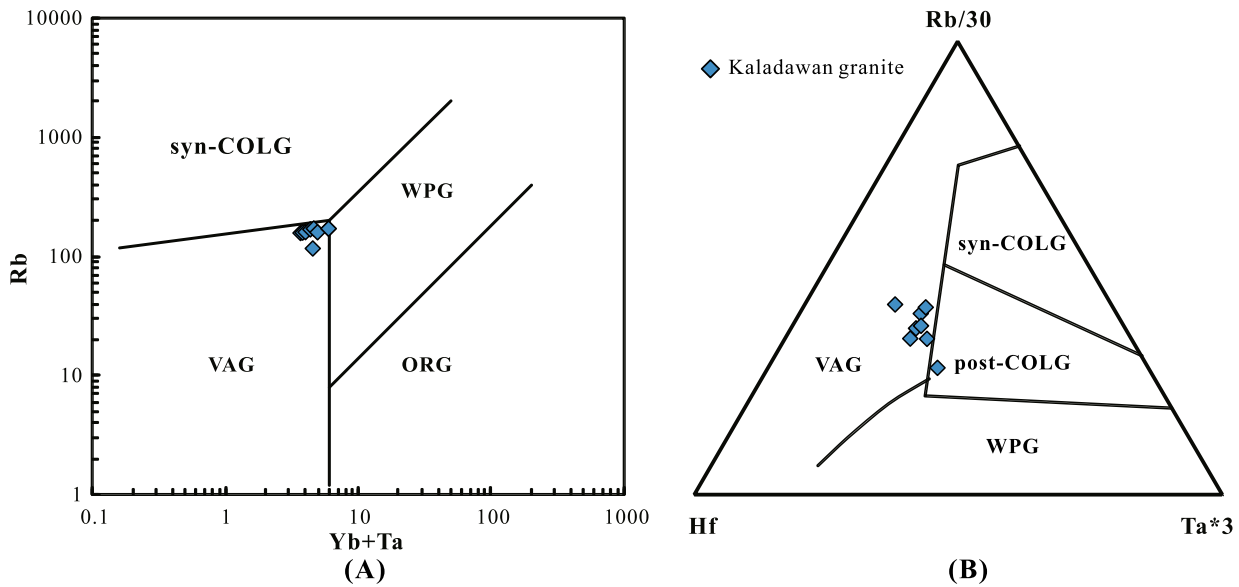


Fig. 14. (A) $(Y + Nb) - Rb$ (Pearce et al., 1984) and (B) $Rb/30 - Hf - 3^*Ta$ (Harris et al., 1986) granite tectonic discrimination diagrams for the Kaladawan granites. Abbreviations: VAG: Volcanic arc granites; ORG: Oceanic ridge granites; WPG: Within-plate granites; Syn-COLG: Syn-collision granites; POG: Post-collision granites.

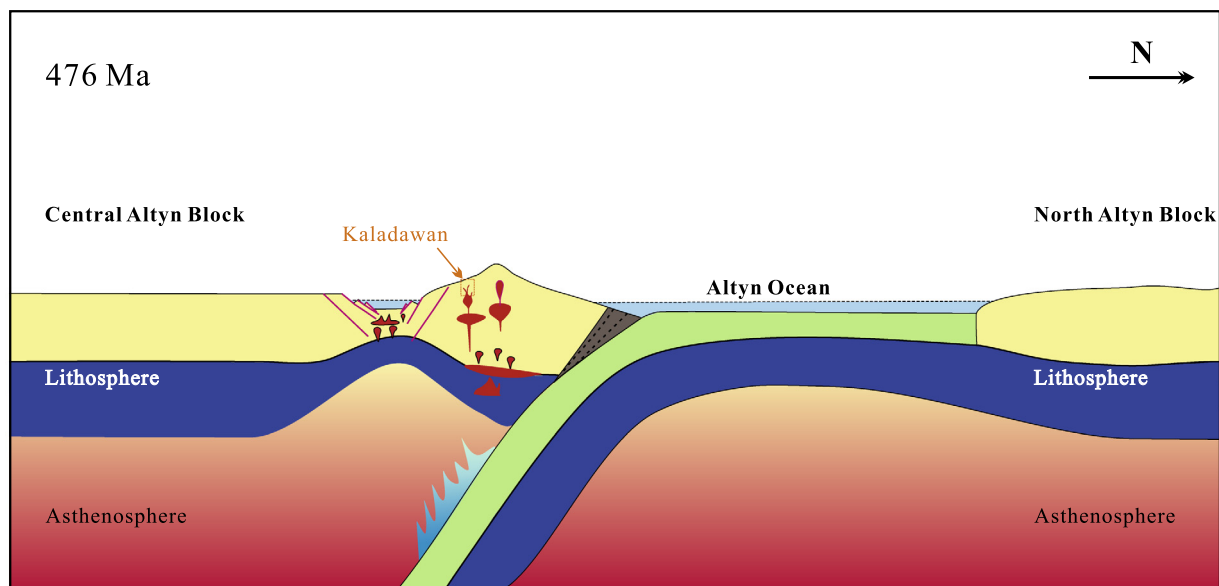


Fig. 15. Schematic tectonic model for the Kaladawan ore field at about 476 Ma.

zircon $\varepsilon_{Hf}(t)$ values and corresponding whole rock $\varepsilon_{Nd}(t)$ of -1.1 , indicating a decoupled Hf–Nd isotopic compositions. (The Hf–Nd isotopic decoupling was possibly caused by the higher solubility of Nd compared to Hf in the slab-derived fluid during an orogenic phase (Kessel et al., 2005; Polat and Münker, 2004; Vervoort and Blichert-Toft, 1999; Woodhead et al., 2001). Minor crustal contamination and/or hydrothermal alteration after zircon crystallization may also have a certain degree of contribution to the Hf–Nd isotopic decoupling in the shallow crust (Farmer and Depaolo, 1987).

6.3. Tectonic and ore genesis implications

Previous studies proposed that an early Paleozoic suture may exist in northern Altnyn based on the presence of ophiolite (zircon SHRIMP U–Pb: 479.4 ± 8.5 Ma; Yang et al., 2008) and high pressure metamorphic rocks such as eclogite (phengite Ar–Ar: ca. 512 Ma) (Che et al., 1995a; Che et al., 1995b; Sobel and Arnaud, 1999;

Zhang et al., 2007), and volcanic rocks with continental arc-related geochemistry were also documented (Cui et al., 2010; Li et al., 2013). Arc-related calc-alkaline granitoids, e.g., the Qiashikansayi granodiorite (481.5 ± 5.3 Ma; Qi et al., 2005), Bashikaogong granite (474.3 ± 6.8 Ma; Wu et al., 2009), and Qilesayi diorite (469.7 ± 3.4 Ma; Zhang et al., 2012) were also reported. These granitoids are largely coeval with the Kaladawan granites (ca. 476 Ma), and are all formed in an active continental margin setting. This interpretation is consistent with the geochemical signatures of the granite, which plot in the volcanic arc granite domain in the Rb vs. $(Yb + Ta)$ and $Rb/30 - Hf - Ta^*3$ tectonic discrimination diagrams (Fig. 14). These arc-related volcanic rocks and granitoids are situated to the south of the ophiolite and thus the suture zone (Fig. 15), indicating that the North Altnyn subduction system was S-dipping.

On the basis of the above discussions, we propose a new genetic model for the Kaladawan Fe–Mo ore field. During the Late

Cambrian to Early Ordovician, the “Altn Ocean” (Chen et al., 2003) was subducted southward beneath the Central Altn block. Continuous subduction may have triggered extensive mafic-intermediate magmatism in the overriding plate and forming the arc volcanic rocks of the Kaladawan Formation (Chen et al., 2016; Cui et al., 2010). The underplating of mafic magma may have caused the partial melting of the lower crust. The mixing of these magmas may have resulted in the development of a felsic magma, which experienced high degrees of fractionation before being emplaced along faults and intruding the ore-hosting Tashibulake Formation. Along and around the intrusive contact, interactions between the granite-derived fluids and the Tashibulake Formation marble may have generated the extensive skarn alteration and the Fe–Mo mineralization.

7. Conclusions

- (1) Granites at the Kaladawan Fe–Mo ore field belong to peraluminous high-K calc-alkaline series, and are highly fractionated I-type.
- (2) The Kaladawan granites were likely formed by fractional crystallization of a parental magma that was derived from the partial melting of a mixture of crustal and mantle materials.
- (3) Deposits in the Kaladawan Fe–Mo field belong to a skarn system and may have formed via contact metamorphism and metasomatic reaction between granite-derived fluids with the wall rocks.
- (4) Deposits in the Kaladawan Fe–Mo ore field were likely formed in an active continental margin.

Acknowledgement

This research was financially supported by the Chinese National Basic Research 973-Program (2014CB440802), Creative and interdisciplinary program, CAS (Y433131A07), Strategic Priority Research Program (B), CAS (XDB1803206), Geological Survey of China (1212011140056), the National Natural Science Foundation of China (41072077) and Knowledge Innovation Program of CAS (40730421). We thank Irs.Wanxiu Qi and Bing Liu (No. 1 Geological Team, Institute of Xinjiang Geological Survey) for the field assistance. We are grateful to Liang Qi, Chunrong Diwu, Le Zhang, Pin Wang, Yanshuang Wu, Weifeng Zhang and Liandang Zhao for the laboratory assistance and manuscript preparation.

References

- Belevtsev, Y.N., 1982. Volcanogenic-sedimentary origin of magnetite ores of the Urals. *Int. Geol. Rev.* 24, 1405–1416.
- Blichert-Toft, J., Albarède, F., 1997. The Lu–Hf isotope geochemistry of chondrites and the evolution of the mantle-crust system. *Earth Planet. Sci. Lett.* 148, 243–258.
- Burton, K.W., Bourdon, B., Birck, J.L., Allègre, C.J., Hein, J.R., 1999. Osmium isotope variations in the oceans recorded by Fe–Mn crusts. *Earth Planet. Sci. Lett.* 171, 185–197.
- Chappell, B.W., 1999. Aluminium saturation in I- and S-type granites and the characterization of fractionated haplogranites. *Lithos* 46, 535–551.
- Chappell, B.W., White, A.J.R., 1992. I- and S-type granites in the Lachlan Fold Belt. *Trans. R. Soc. Edinburgh: Earth Sci.* 83, 1–26.
- Che, Z.C., Liu, L., Liu, H.F., Luo, J.H., 1995a. Discovery and occurrence of high-pressure metapelitic rocks from Altun Mountain areas, Xinjiang autonomous region. *China Sci. Bull.* 40, 1298–1300 (in Chinese with English abstract).
- Che, Z.C., Liu, L., Sun, Y., 1995b. U–Pb, Sr–Nd, Rb–Sr, $^{40}\text{Ar}/^{39}\text{Ar}$ and $^{18}\text{O}/^{16}\text{O}$ isotopic studies for early evolution of the structural belt in the Altun area. *Acta Geosci. Sin.* 03, 334–337 (in Chinese with English abstract).
- Chen, B.L., Jiang, R.B., Li, L., Chen, Z.L., Qi, W.X., Liu, R., Cui, L.L., Wang, S.X., 2009. Discovery of iron ore zone in the Kaladawan Area within the eastern part of the Altun Mountains and its significance. *Acta Geosci. Sin.* 30, 143–154 (in Chinese with English abstract).
- Chen, B., Li, S., Jiang, R., Chen, Z., Han, F., Cui, L., Li, L., Zhao, S., Qi, W., Yang, Y., Wang, S., Wang, Y., Zhou, Y., Hao, R., 2016. Zircon SHRIMP U–Pb dating of intermediate-felsic volcanic rocks from the Kaladawan area, Altun Mountains and its tectonic environment. *Acta Geol. Sin.* 90, 708–727 (in Chinese with English abstract).
- Chen, X., Wang, X., Yang, F., Chen, Z., Chen, B., Wang, K., 2001. Tectonic environments of magmatism in Early Paleozoic in the North Altn Tagh, China. *J. Geomech.* 7, 193–200 (in Chinese with English abstract).
- Chen, X.H., Yin, A., Gehrels, G.E., Cowgill, E.S., Grove, M., Harrison, T.M., Wang, X.F., 2003. Two phases of Mesozoic north-south extension in the eastern Altn Tagh range, northern Tibetan Plateau. *Tectonics* 22, 1053–1074.
- Chen, Y., Dai, J.Y., Li, G., An, L.X., 2012. The geological characteristics of Kaladawan iron deposit and its prospecting criterias. *Xinjiang Nonferrous Met.* 1 (S2), 1–3 (in Chinese with English abstract).
- Coleman, R.G., Donato, M.M., 1979. Oceanic plagiogranite. *Dev. Petrol.* 6, 149–168.
- Cui, L.L., Chen, B.L., Yong, N., Chen, Z.L., Ding, W.J., 2010. Geochemistry and genesis of basic-intermediate volcanic rocks from Kaladawan, east Altn Tagh mountain. *J. Geomech.* 16, 96–107 (in Chinese with English abstract).
- Deng, X.H., Chen, Y.J., Santosh, M., Zhao, G.C., Yao, J.M., 2013. Metallogeny during continental outgrowth in the Columbia supercontinent: isotopic characterization of the Zhaiwa Mo–Cu system in the North China Craton. *Ore Geol. Rev.* 51, 43–56.
- Dill, H.G., 2010. The “chessboard” classification scheme of mineral deposits: mineralogy and geology from aluminum to zirconium. *Earth-Sci. Rev.* 100, 1–420.
- Einaudi, M.T., Meinert, L.D., Newberry R.T., 1981. Skarn deposits. *Econ. Geol.* 75th Ann. Vol. 317–391.
- Farmer, G.L., DePaolo, D.J., 1987. Nd and Sr isotope study of hydrothermally altered granite at San Manuel, Arizona; implications for element migration paths during the formation of porphyry copper ore deposits. *Econ. Geol.* 82, 1142–1151.
- Gao, X.F., Xiao, P.X., Kang, L., Guo, L., Dong, Z.C., Xi, R.G., 2012. The origin of volcanic rocks in the Kaladawan iron ore district of eastern Altun Mountains and its geological and metallogenic significance. *Geol. Bull. China* 31, 2070–2075 (in Chinese with English abstract).
- Govindaraju, K., 1994. 1994 compilation of working values and sample description for 383 geostandards. *Geostand. Newsl.* 18, 1–158.
- Griffin, W.L., Pearson, N.J., Belousova, E., Jackson, S.E., Van Acherbergh, E., O’Reilly, S.Y., Shee, S.R., 2000. The Hf isotope composition of cratonic mantle: LAM–MC–ICPMS analysis of zircon megacrysts in kimberlites. *Geochim. Cosmochim. Acta* 64, 133–147.
- Griffin, W.L., Wang, X., Jackson, S.E., Pearson, S.E., O’Reilly, S.Y., Xu, X.S., Zhou, X.M., 2002. Zircon chemistry and magma genesis, SE China: In-situ analysis of Hf isotopes, Tonglu and Pingtan igneous complexes. *Lithos* 61, 237–269.
- Han, F.B., Chen, B.L., Cui, L.L., Yong, N., Chen, Z.L., Ding, W.J., 2012. Zircon SHRIMP U–Pb age of intermediate–acid intrusive rocks in Kaladawan area, eastern Altun Mountains, NW China, and its implications. *Acta Petrol. Sin.* 028, 2277–2291.
- Hao, R.X., 2013. The Characteristics and Genetic of Kaladawan Area Iron Deposit, Altn Tagh, Xinjiang (Master thesis). Chinese Academy of Geological Sciences, Beijing, pp. 1–89 (in Chinese with English abstract).
- Harris, N.B., Pearce, J.A., Tindle, A.G., 1986. Geochemical characteristics of collision-zone magmatism. *Geol. Soc. London Special Publications* 19, 67–81.
- Hou, T., Zhang, Z.C., Pirajno, F., Santosh, M., Encarnacion, J., Liu, J.L., Zhao, Z.D., Zhang, L.J., 2014a. Geology, tectonic settings and iron ore metallogenesis associated with submarine volcanism in China: an overview. *Ore Geol. Rev.* 57, 498–517.
- Hou, T., Zhang, Z., Santosh, M., Encarnacion, J., Zhu, J., Luo, W., 2014b. Geochronology and geochemistry of submarine volcanic rocks in the Yamansu iron deposit, Eastern Tianshan Mountains, NW China: constraints on the metallogenesis. *Ore Geol. Rev.* 56, 487–502.
- Jacobsen, S.B., Wasserburg, G.J., 1980. Sm–Nd isotopic evolution of chondrites. *Earth Planet. Sci. Lett.* 50, 139–155.
- Kessel, R., Schmidt, M.W., Ulmer, P., Pettker, T., 2005. Trace element signature of subduction-zone fluids, melts and supercritical liquids at 120–180 km depth. *Nature* 437, 724–727.
- Li, N., Ulrich, T., Chen, Y.J., Thompson, T.B., Peace, V., Pirajno, F., 2012. Fluid evolution of the Yuchiling porphyry Mo deposit, East Qinling, China. *Ore Geol. Rev.* 48, 442–459.
- Li, S.B., Chen, B.L., Chen, Z.L., Hao, R.X., Zhou, Y.G., Han, F.B., 2013. Geochemistry and tectonic implications of the Early Paleozoic felsic to intermediate volcanic rocks from Kaladawan Area, North Altn. *Geol. Rev.* 59, 423–436 (in Chinese with English abstract).
- Li, X., Li, W., Li, Z.X., 2007. On the genetic classification and tectonic implications of the Early Yanshanian granitoids in the Nanling Range, South China. *Chin. Sci. Bull.* 52, 1873–1885.
- Li, X.H., Long, W.G., Li, Q.L., Liu, Y., Zheng, Y.F., Yang, Y.H., Chamberlain, K.R., Wan, D. F., Guo, C.H., Wang, X.C., 2010. Penglai zircon megacrysts: a potential new working reference material for microbeam determination of Hf–O isotopes and U–Pb age. *Geostand. Geoanal. Res.* 34, 117–134.
- Liu, Y.S., Hu, Z.C., Gao, S., Günther, D., Xu, J., Gao, C.G., Chen, H.H., 2008. In situ analysis of major and trace elements of anhydrous minerals by LA-ICP-MS without applying an internal standard. *Chem. Geol.* 257, 34–43.
- Lugmair, G.W., Marti, K., 1978. Lunar initial $^{143}\text{Nd}/^{144}\text{Nd}$: differential evolution of the lunar crust and mantle. *Earth Planet. Sci. Lett.* 39, 349–357.
- Mao, J., Xie, G., Duan, C., Pirajno, F., Ishiyama, D., Chen, Y., 2011. A tectono-genetic model for porphyry-skarn-stratabound Cu–Au–Mo–Fe and magnetite-apatite

- deposits along the Middle-Lower Yangtze River Valley, Eastern China. *Ore Geol. Rev.* 43, 294–314.
- Meinert, L.D., Dipple, G.M., Nicolescu, S., 2005. World skarn deposits. *Econ. Geol.* 100th Anniv. Vol. 299–336.
- Meng, L., Chen, B., Luo, D., Wang, Y., Sun, Y., Wu, Y., Zhang, H., Wang, T., 2015. SHRIMP zircon U-Pb geochronology of northern Highland 4337 granodiorite in Kaladawan area of northern Altun Mountains and its tectonic implications. *J. Jilin Univ. (Earth Science Edition)* 45, 1757–1771 (in Chinese with English abstract).
- Nowell, G.M., Kempton, P.D., Noble, S.R., Fitton, J.G., Saunders, A.D., Mahoney, J.J., Taylor, R.N., 1998. High precision Hf isotope measurements of MORB and OIB by thermal ionisation mass spectrometry: insights into the depleted mantle. *Chem. Geol.* 149, 211–233.
- Pan, Y., Dong, P., 1999. The lower Changjiang (Yangzi/Yangtze River) metallogenic belt, east central China: Intrusion- and wall rock-hosted Cu-Fe-Au, Mo, Zn, Pb, Ag deposits. *Ore Geol. Rev.* 15, 177–242.
- Pearce, J.A., Harris, N.B., Tindle, A.G., 1984. Trace element discrimination diagrams for the tectonic interpretation of granitic rocks. *J. Petrol.* 25, 956–983.
- Pearce, J.A., Norry, M.J., 1979. Petrogenetic implications of Ti, Zr, Y, and Nb variations in volcanic rocks. *Contrib. Mineral. Petrol.* 69, 33–47.
- Pearce, J.A., Peate, D.W., 1995. Tectonic implications of the composition of volcanic arc magmas. *Annu. Rev. Earth Planet. Sci.* 23, 251–285.
- Peucat, J.J., Vidal, P., Bernard-Griffiths, J., Condie, K.C., 1988. Sr, Nd and Pb isotopic systematics in the Archean low- to high-grade transition zone of southern India: syn accretion vs. post-accretion granites. *J. Geol.* 97, 537–550.
- Pitcher, W.S., 1982. Granite type and tectonic environment. In: Hsu, K.J. (Ed.), *Mountain Building Processes*. Academic Press, London, pp. 19–40.
- Polat, A., Münker, C., 2004. Hf-Nd isotope evidence for contemporaneous subduction processes in the source of late Archean arc lavas from the Superior Province, Canada. *Chem. Geol.* 213, 403–429.
- Pons, J.M., Franchini, M., Meinert, L., Recio, C., Etcheverry, R., 2009. Iron Skarns of the Vegas Peladas District, Mendoza, Argentina. *Econ. Geol.* 104, 157–184.
- Qi, L., Hu, J., Gregoire, D.C., 2000. Determination of trace elements in granites by inductively coupled plasma mass spectrometry. *Talanta* 51, 507–513.
- Qi, X.X., Li, H.B., Wu, C.L., Yang, J.S., Zhang, J.X., Meng, F.C., Shi, D.R., Chen, S.Y., 2005. Zircon SHRIMP U-Pb dating of the Qiashikansayi granodiorite from North Altyn and its geological significances. *Sci. Bull.* 50, 571–576 (in Chinese with English abstract).
- Salters, V.J.M., Stracke, A., 2004. Composition of the depleted mantle. *Geochem. Geophys. Geosyst.* 5. <http://dx.doi.org/10.1029/2003GC000597>.
- Scherer, E., Münker, C., Mezger, K., 2001. Calibration of the lutetium–hafnium clock. *Science* 293, 683–687.
- Sobel, E.R., Arnaud, N., 1999. A possible middle Paleozoic suture in the Altyn Tagh, NW China. *Tectonics* 18, 64–74.
- Steiger, R.H., Jäger, E., 1977. Subcommission on geochronology: convention of the use of decay constants in geo- and cosmochronology. *Earth Planet. Sci. Lett.* 36, 359–362.
- Stern, R.J., Fouch, M.J., Klempner, S.L., 2003. An overview of the Izu-Bonin-Mariana subduction factory. In: *Inside the Subduction Factory*. AGU, Washington, DC, pp. 175–222.
- Sun, S.S., McDonough, W.F., 1989. Chemical and isotopic systematics of oceanic basalts: implication for the mantle composition and process. In: Saunderson, A.D., Norry, M.J. (Eds.), *Magmatism in the Ocean Basins*, 42. Geological Society of London Special Publication, pp. 313–345.
- Vervoort, J.D., Blichert-Toft, J., 1999. Evolution of the depleted mantle: Hf isotope evidence from juvenile rocks through time. *Geochim. Cosmochim. Acta* 63, 533–556.
- Wan, B., Xiao, W., Zhang, L., Han, C., 2012. Iron mineralization associated with a major strike-slip shear zone: radiometric and oxygen isotope evidence from the Mengku deposit, NW China. *Ore Geol. Rev.* 44, 136–147.
- Wan, B., Xiao, W., Windley, B.F., Gao, J., Zhang, L., Cai, K., 2017. Contrasting ore styles and their role in understanding the evolution of the Altoids. *Ore Geol. Rev.* 80, 910–922.
- Wang, C.M., Zhang, L., Tang, H.-S., Chen, H.Y., Li, X.L., Zheng, Y., Li, D.F., Fang, J., Dong, L.H., Qu, X., 2017. Genesis of the Kaladawan Fe–Mo ore field in Altyn, Xinjiang, China: constraints from mineralogy and geochemistry. *Ore Geol. Rev.* 81, 587–601.
- Wang, C.M., Zhang, L., Chen, H.Y., Zheng, Y., Li, D.F., Fang, J., 2014. Ore geology and fluid inclusion characteristics of the Kaladawan Skarn Fe–Mo Deposit in North Altun Tagh, Northwest China. *Acta Geol. Sin.* 88, 383–384.
- Weis, D., Kieffer, B., Maerschalk, C., Barling, J., De Jong, J., Williams, G.A., Hanano, D., Pretorius, W., Mattielli, N., Scoates, J.S., Goolaerts, A., Friedman, R.M., Mahoney, J.B., 2006. High-precision isotopic characterization of USGS reference materials by TIMS and MC-ICP-MS. *Geochem. Geophys. Geosyst.* 7.
- Whalen, J.B., Currie, K.L., Chappell, B.W., 1987. A-type granites: geochemical characteristics, discrimination and petrogenesis. *Contrib. Mineral. Petrol.* 95, 407–419.
- Woodhead, J., Hergt, J., Davidson, J., Eggins, S., 2001. Hafnium isotope evidence for 'conservative' element mobility during subduction zone processes. *Earth Planet. Sci. Lett.* 192, 331–346.
- Wu, C.L., Yang, J.S., Robinson, P.T., Wooden, J.L., Mazdab, F.K., Gao, Y.H., Wu, S.P., Chen, Q.L., 2009. Geochemistry, age and tectonic significance of granitic rocks in north Altun, northwest China. *Lithos* 113, 423–436.
- Wu, F.Y., Jahn, B.M., Wilde, S.A., Lo, C.H., Yui, T.F., Lin, Q., Ge, W.C., Sun, D.Y., 2003. Highly fractionated I-type granites in NE China (II): isotopic geochemistry and implications for crustal growth in the Phanerozoic. *Lithos* 67, 191–204.
- Wu, F.Y., Yang, Y.H., Xie, L.W., Yang, J.H., Xu, P., 2006. Hf isotopic compositions of the standard zircons and baddeleyites used in U-Pb geochronology. *Chem. Geol.* 234, 105–126.
- Xin, H.T., 2012. The Chronotectonic Framework and Main Geological Events of Early Precambrian in the Agetashtage Area, Southeastern Margin of Tarim Basin (Ph. D. thesis). China University of Geosciences, Beijing, pp. 1–127 (in Chinese with English abstract).
- Yang, J.S., Shi, D.R., Wu, C.L., Su, D.C., Chen, S.Y., Wang, X.B., Wooden, J., 2008. Petrology and SHRIMP age of the Hongliugou ophiolite at Milan, north Altun, at the northern margin of Tibetan plateau. *Acta Petrol. Sin.* 024, 1567–1584 (in Chinese with English abstract).
- Yang, Y., Chen, Y.J., Zhang, J., Zhang, C., 2013. Ore geology, fluid inclusions and four-stage hydrothermal mineralization of the Shangfanggou giant Mo–Fe deposit in Eastern Qinling, central China. *Ore Geol. Rev.* 55, 146–161.
- Zhai, Y.S., Xiong, Y.L., Yao, S., Lin, X., 1996. Metallogeny of copper and iron deposits in the Eastern Yangtse Craton, east-central China. *Ore Geol. Rev.* 11, 229–248.
- Zhang, J.X., Meng, F.C., Yu, S.Y., Chen, W., Chen, S.Y., 2007. ⁴⁰Ar/³⁹Ar geochronology of high-pressure/low-temperature blueschists and eclogites in the North Altyn Tagh and their tectonic implications. *Geol. China* 34, 558–564 (in Chinese with English abstract).
- Zhang, Z.C., Hou, T., Santosh, M., Li, H., Li, J., Zhang, Z., Song, X., Wang, M., 2014. Spatio-temporal distribution and tectonic settings of the major iron deposits in China: an overview. *Ore Geol. Rev.* 57, 247–263.
- Zhang, Z.W., Li, G., Li, H.M., Zhang, W.F., 2012. LA-ICP-MS zircon U-Pb geochronology and geochemistry of gabbro and diorite from Qilesayi pluton in Lapeiquan area of northern Altun Mountains and their tectonic implications. *Acta Petrol. Mineral.* 31, 13–27 (in Chinese with English abstract).
- Zheng, Y., Chen, Y., Dai, L., Zhao, Z., 2015. Developing plate tectonics theory from oceanic subduction zones to collisional orogens. *Sci. China, Ser. D Earth Sci.* 58, 1045–1069 (in Chinese with English abstract).